Anisotropic energy transfers in rotating turbulence

Cyril Lamriben, Pierre-Philippe Cortet, Frédéric Moisy
Laboratoire FAST, CNRS, Univ Paris-Sud, UPMC Univ Paris 06, Bât. 502, Campus universitaire, 91405 Orsay, France

Abstract.
We investigate experimentally the anisotropic energy transfers in freely decaying turbulence subjected to a background rotation. The energy distribution $E(\mathbf{r},t) = \langle(\delta\mathbf{u})^2\rangle$ and the anisotropic energy flux density $\mathbf{F}(\mathbf{r}) = \langle\delta\mathbf{u}\,(\delta\mathbf{u})^2\rangle$, where $\delta\mathbf{u}$ is the vector velocity increment over separation $\mathbf{r}$, are determined from large data sets of Particle Image Velocimetry measurements. Surprisingly, although $E(\mathbf{r})$ is strongly anisotropic at all scales, $\mathbf{F}(\mathbf{r})$ remains almost radial, except in the near-dissipative range. The anisotropy growth of decaying rotating turbulence is therefore proved to be essentially driven by a nearly radial, but orientation-dependent, energy flux density $\mathbf{F}(\mathbf{r})$.

1. Introduction

The description of the energy transfers from large to small scales by the Kolmogorov 4/5th law is often considered as the most fundamental result of homogeneous and isotropic turbulence theory (1; 2). In the presence of a background rotation, a situation which is relevant for most geophysical and astrophysical flows, the addition of the Coriolis force makes these energy transfers anisotropic, resulting in a gradual columnar structuring of the turbulence along the rotation axis (3; 4; 5). In the limit of large rotation rates, turbulence even tends to become two-dimensional —but still three-component (2D-3C)—, in agreement with the Taylor-Proudman theorem. Although the resulting anisotropic energy distribution has been characterized numerically and experimentally (6; 7), direct evidence of the anisotropy of the physical-space energy transfers accounting for this non-trivial flow organization under rotation is still lacking.

For homogeneous but not necessarily isotropic turbulence, the energy distribution and energy flux density in the space of separations $\mathbf{r}$ are described by the fields

$$E(\mathbf{r},t) = \langle(\delta\mathbf{u})^2\rangle \qquad \text{and} \qquad \mathbf{F}(\mathbf{r},t) = \langle\delta\mathbf{u}\,(\delta\mathbf{u})^2\rangle, \tag{1}$$

where $\mathbf{u}(\mathbf{x},t)$ is the turbulent velocity field, $\delta\mathbf{u} = \mathbf{u}(\mathbf{x}+\mathbf{r},t) - \mathbf{u}(\mathbf{x},t)$ the velocity vector increment over $\mathbf{r}$ (see Fig. 1), and where $\langle\cdot\rangle$ denotes spatial and ensemble averages. The temporal evolution of the energy distribution in the physical space is governed by the Kármán-Howarth-Monin (KHM) equation (1; 8),

$$\frac{1}{2}\frac{\partial}{\partial t}R = \frac{1}{4}\nabla\cdot\mathbf{F} + \nu\nabla^2 R, \tag{2}$$

where $R(\mathbf{r},t) = \langle \mathbf{u}(\mathbf{x},t)\cdot\mathbf{u}(\mathbf{x}+\mathbf{r},t)\rangle = \langle \mathbf{u}^2\rangle - E(\mathbf{r},t)/2$ is the two-point velocity correlation and ν the kinematic viscosity. Importantly, this equation is still valid for homogeneous anisotropic turbulence (9), and in particular for axisymmetric turbulence in a rotating frame.

For stationary (forced) turbulence, this equation reduces to $\nabla\cdot\mathbf{F} = -4\,\epsilon$ in the inertial range, where ϵ stands for the rates of injected and dissipated energy. In the isotropic case, this constant-flux relation can be integrated, yielding a purely radial flux density, $\mathbf{F}(\mathbf{r}) = -(4/3)\,\epsilon\,\mathbf{r}$, that describes the usual energy cascade from large to small scales. This result is actually identical to the celebrated Kolmogorov's 4/5th law, classically expressed in terms of the 3rd order longitudinal structure function, $\langle \delta u_L^3\rangle = -(4/5)\,\epsilon\, r$, where $\delta u_L = \delta\mathbf{u}\cdot\mathbf{r}/r$ is the longitudinal velocity increment.

In decaying rotating homogeneous turbulence, Eq. (2) shows that, starting from an isotropic initial energy distribution $E(\mathbf{r},0)$, an anisotropy growth in $E(\mathbf{r},t)$ is expected if an anisotropic energy flux $\nabla\cdot\mathbf{F}$ is induced by the Coriolis force. However, the flux density $\mathbf{F}(\mathbf{r})$ itself has never been measured, and its precise form, which reveals the fundamental action of rotation on turbulence, is so far unknown. To date, the only experimental attempts to characterize the energy transfers in rotating turbulence were restricted to measurements of $\langle \delta u_L^3\rangle$ in the plane normal to the rotation axis (10; 11), hence ignoring the anisotropic nature of those transfers. Recent theoretical efforts have been made to generalize the 4/5th law, assuming weak anisotropy (12), or considering the full anisotropic problem (2) but restricted to the stationary case (9).

The aim of the present work is to provide direct experimental measurements, in the physical space, of the energy distribution $E(\mathbf{r},t) = \langle \delta\mathbf{u}^2\rangle$ and of the energy transfer density $\mathbf{F}(\mathbf{r},t)$ in homogenous decaying turbulence, with and without background rotation.

2. Experiments

The experimental setup (Fig. 1(a)) is described in details in Ref. (13). Turbulence is generated by rapidly towing a grid (velocity $V_g = 1.0$ m.s^{-1}, mesh size $M = 40$ mm) in a square water tank mounted on a rotating platform. Velocity fields are measured in a vertical plane (12×12 cm^2 field of view) in the rotating frame using a corotating Particle Image Velocimetry system. Runs for three rotation rates, $\Omega = 0.42, 0.84$ and 1.68 rad s^{-1} (4, 8 and 16 rpm respectively), as well as a reference run without rotation, have been carried out. The Reynolds number based on the grid mesh is $Re_g = V_g M/\nu = 40\,000$, and the Rossby number $Ro_g = V_g/2\Omega M$ ranges from 7.4 to 30, indicating that the flow in the close wake of the grid is fully turbulent and weakly affected by rotation. An important concern about grid turbulence experiments in a confined rotating volume is the excitation of reproducible inertial modes (14). Here, we use the modified grid configuration introduced in Ref. (13), which was shown to significantly reduce the generation of these inertial modes.

During the decay of turbulence, 60 image pairs are acquired by a double-frame 2048^2 pixels camera, at a rate of 1 image pair per second. The PIV resolution, $\Delta x = 1.3$ mm, is sufficient to resolve the inertial range but fails to resolve the dissipative scale (the Kolmogorov scale is of the order of 0.2 mm right after the grid translation (11)).

From the measured 2D velocity fields, only surrogates of the energy distribution and flux density (1) can be computed, namely

$$\widetilde{E}(\mathbf{r}) = \langle \delta u_x^2 + \delta u_z^2\rangle_{x,z}, \quad \widetilde{\mathbf{F}}(\mathbf{r}) = \langle \delta\mathbf{u}(\delta u_x^2 + \delta u_z^2)\rangle_{x,z}, \tag{3}$$

where the spatial average is restricted to the measurement plane, and $\mathbf{r} = r_x\mathbf{e}_x + r_z\mathbf{e}_z$. For each time after the grid translation, these quantities are computed for all separations $\mathbf{r}$ lying in the PIV field of view, and are ensemble-averaged over 600 realizations of the turbulence decay. The fields $\widetilde{E}(\mathbf{r})$ and $\widetilde{\mathbf{F}}(\mathbf{r})$ are remapped on a spherical coordinate system (r,θ,ϕ), where $r = |\mathbf{r}|$,

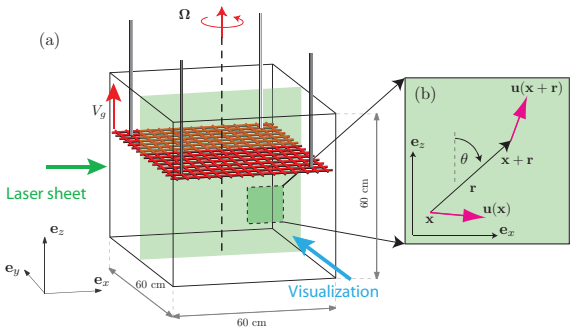

Figure 1. (a) Experimental setup: $(60\text{ cm})^3$ tank filled with 52 cm of water and rotating at $0 \leq \Omega \leq 1.68$ rad s^{-1}. The grid is towed from the bottom to the top, and PIV measurements are performed in the vertical plane (x, z) in the rotating frame during the turbulence decay. (b) Definition of the vector velocity increment $\delta\mathbf{u} = \mathbf{u}(\mathbf{x}+\mathbf{r}) - \mathbf{u}(\mathbf{x})$.

and θ is the polar angle between $\mathbf{e}_z$ and $\mathbf{r}$; the invariance with respect to the (non-measured) azimuthal angle ϕ is assumed by axisymmetry. Although relations between the surrogates (3) and the exact 3-components quantities (1) can be derived for isotropic turbulence, no general relation holds in the anisotropic case. Therefore, we do not apply any correction weight when computing $\widetilde{E}$ and $\widetilde{\mathbf{F}}$, and we drop the tildes $\widetilde{\cdot}$ in the following.

3. Statistics convergence

The convergence of the statistics from experimental measurements is very delicate to achieve, in particular for the computation of the energy flux density $\mathbf{F}(\mathbf{r})$, which is a 3rd order moment of a zero-mean velocity increment. To evaluate the level of convergence of a measured quantity $X(\mathbf{r})$ (with $X(\mathbf{r}) = \mathbf{E}(\mathbf{r})$ or $X(\mathbf{r}) = |\mathbf{F}(\mathbf{r})|$), we split our sample of 600 realizations at a given time into eight independant sub-samples of equal size, and compute for each sub-sample the corresponding average $X_i(\mathbf{r})$ for all separations $\mathbf{r}$. The standard deviation $\sigma\{X_i(\mathbf{r})\}$ around the mean $\overline{X}(\mathbf{r})$ of these eight sub-samples provides an estimate of the absolute error on $X(\mathbf{r})$ when computed over 75 independant realizations. We define the relative error $\varepsilon_X(r)$ for a given quantity $X(\mathbf{r})$ as the ratio of $\sigma\{X_i(\mathbf{r})\}$, averaged over θ, to the maximum value obtained over all separations $\mathbf{r}$ of $\overline{X}(\mathbf{r})$:

$$\varepsilon_X(r) = \frac{\langle \sigma\{X_i(r)\}\rangle_\theta}{\max\limits_{\mathbf{r}} \left(\overline{X}(\mathbf{r})\right)} \tag{4}$$

Normalizing the absolute error by $\max\limits_{\mathbf{r}} \left(\overline{X}(\mathbf{r})\right)$ instead of $\overline{X}(\mathbf{r})$ is a convenient way to ensure that the relative error will not artificially increase with r when considering a quantity tending towards zero at small or large scales. Since the maximum value of $\overline{X}(\mathbf{r})$ is calculated over all separations $\mathbf{r}$, the relative error depends a priori on the choice of the largest separation r_{max} when computing $\varepsilon_X(r)$. In order to reduce this bias, r_{max} is chosen sufficiently large so that $E(\mathbf{r})$ and $|\mathbf{F}(\mathbf{r})|$ reach their maxima at scales smaller than r_{max}.

In Fig. 2, we plot the relative errors ε_E and $\varepsilon_{|F|}$ as functions of the separation r. As expected, the relative error on $|\mathbf{F}|$ (3rd order moment of the velocity increment) is larger than the one on the energy (2nd order moment). The uncertainty on $|\mathbf{F}(\mathbf{r})|$ is better than 10% at small scales but reaches about 20% at scales $r \simeq M$ while an uncertainty better than 4% can be achieved at all scales for the energy. Furthermore, Fig. 2 shows an increase of the relative error with r for both quantities. Indeed, because of the finite size of the velocity field, the number of velocity vectors separated by r which can be considered when computing moment decreases with r, resulting in a larger noise level on $E(\mathbf{r})$ and $|\mathbf{F}(\mathbf{r})|$.

We can conclude that using a set of 600 independent realizations of the turbulence decay (which represents 24 hours of continuous run for each value of Ω) provides well-converged

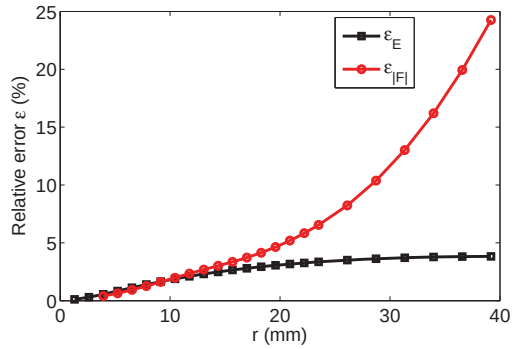

Figure 2. Evolution of the relative error on the energy and on the energy flux density with the separation r at time $t\,V_g/M = 400$ ($t = 16$ s) for $\Omega = 1.68$ rad s^{-1} (16 rpm).

calculations of the energy and of its density flux at small scales, but statistics at scales larger than the mesh size must be considered with caution. However, being additionally more sensitive to remaining inhomogeneities of the flow, those scales larger than M are not considered in the following.

4. Energy distribution

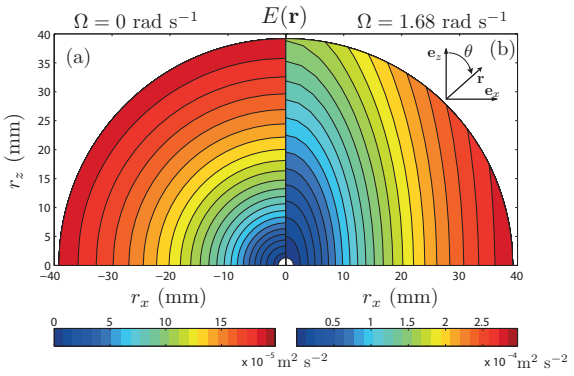

Figure 3. Map of the energy distribution $E(\mathbf{r})$ at a time $t\,V_g/M = 400$ after the grid translation, for (a) $\Omega = 0$, and (b) $\Omega = 1.68$ rad s^{-1} (16 rpm).

Soon after the grid translation, the energy, as measured by the variance of the velocity increments $E(\mathbf{r})$, shows a nearly isotropic distribution with respect to the separation vector $\mathbf{r}$, both in the rotating and non-rotating cases. Fig. 3 (a) shows that, at dimensionless time $t\,V_g/M = 400$ after the grid translation, the iso-E curves remain nearly circular for $\Omega = 0$, reflecting the persistance of isotropy in this case. On the other hand, for $\Omega = 16$ rpm and at the same time after the grid translation, E has developed a strong anisotropy, with a marked depletion along the vertical axis z. The depletion of $E(\mathbf{r})$ corresponds to an enhanced velocity correlation $R(\mathbf{r})$ along the rotation axis, showing a trend towards an invariant 2D-3C flow along the rotation axis, in agreement with the Taylor-Proudman theorem.

5. Energy transfers

We now turn to the energy flux density, and we first present in Fig. 4(a) measurements of $\mathbf{F}(\mathbf{r})$ for $\Omega = 0$, at the same dimensionless time $tV_g/M = 400$. This vector field is found remarkably radial, pointing towards the origin, giving direct evidence of the isotropic energy cascade in the physical space, from the large to the small scales, in the non-rotating case. The isotropy of the flux density magnitude is not as good: the iso-$|\mathbf{F}|$ curves (Fig. 4(b)) are nearly circular up to

$r \simeq 30$ mm, but shows slight departure from isotropy at larger r, suggesting that this quantity is very sensitive to a residual anisotropy of the large-scale flow.

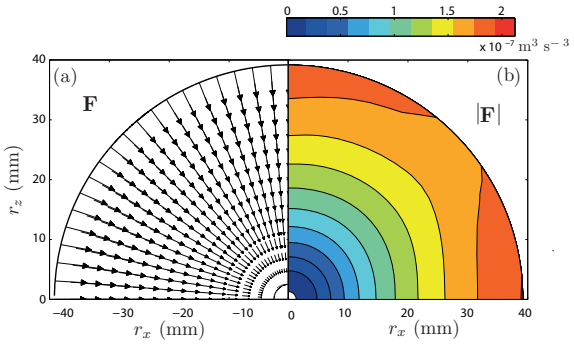

Figure 4. (a) Map of the vector field $\mathbf{F}(\mathbf{r})$ at a time $t\,V_g/M = 400$ after the grid translation, for $\Omega = 0$ rpm. (b) Map of $|\mathbf{F}(\mathbf{r})|$.

We consider now the energy transfers in the rotating case, shown in Fig. 5 (a) at the same time $t\,V_g/M = 400$. Surprisingly, the flux density $\mathbf{F}$ is found to remain nearly radial for all separations, except at the smallest scales, for $r < 10$ mm, where a marked deflection towards the rotation axis is observed. Such horizontally tilted $\mathbf{F}$ is indeed consistent with an asymptotic 2D-3C flow, for which $\mathbf{F}$ must be a strictly horizontal vector, function of the horizontal component of the separation only. If we focus on the flux density magnitude $|\mathbf{F}|$, a clear anisotropy is now found at all scales. The maximum of $|\mathbf{F}|$ is systematically encountered near the rotation axis, at rather large scales, centered around 50-80 mm (outside the range shown in Fig. 5b). The local maximum of $|\mathbf{F}|$ on the horizontal axis is encountered at smaller scales, as evidenced by the crest line of $|\mathbf{F}|$ in Fig. 5(b). This proves that the anisotropy of the energy transfers is mostly driven by the θ-dependence of the radial component F_r, and not by the growth of a nonzero polar component $F_\theta = \mathbf{F} \cdot \mathbf{e}_\theta$.

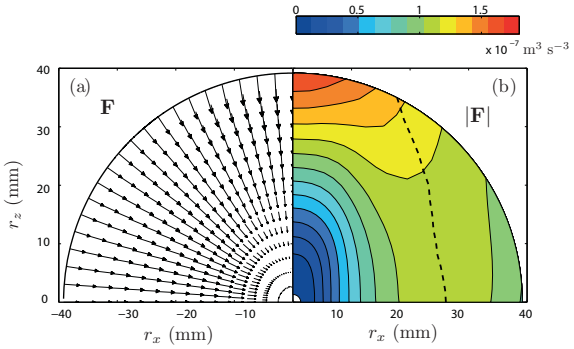

Figure 5. (a) Map of the vector field $\mathbf{F}(\mathbf{r})$ at a time $t\,V_g/M = 400$ after the grid translation, for $\Omega = 16$ rpm. (b) Map of $|\mathbf{F}(\mathbf{r})|$.

6. Conclusion

We report the first direct measurements of the energy flux density $\mathbf{F}$ in the physical space in a decaying rotating turbulence experiment. Although the alternative description of the energy transfers in the spectral space is more natural for theory or numerics (2; 3; 4; 6), the direct use of the KHM equation (2) in the physical space, which is better suited for experiments, reveals here new and unexpected behaviors. Surprisingly, the anisotropy growth of the energy distribution is primarily driven by an almost radial, but orientation-dependent, flux density $\mathbf{F}$, except at small scales where $\mathbf{F}$ shows a horizontal tilt, compatible with a trend towards a 2D state. The reported results should motivate new theoretical efforts to describe the rotation-induced structuring of the physical-space energy flux density.

We acknowledge S. Galtier, J.-P. Hulin, and M. Rabaud for fruitful discussions, and Triangle de la Physique for the funding of the "Gyroflow" rotating platform.

References

[1] Frisch, U. 1995 *Turbulence - The Legacy of A. N. Kolmogorov* Cambrige University Press, London.

[2] Sagaut, P. & Cambon, C. 2008 *Homogeneous Turbulence Dynamics* Cambridge University Press, London.

[3] Cambon, C. & Jacquin, L. 1989 Spectral approach to non-isotropic turbulence subjected to rotation *J. Fluid Mech.* **202**, 295.

[4] Waleffe, F. 1993 Inertial transfers in the helical decomposition *Phys. Fluids A* **5**, 677.

[5] Staplehurst, P.J., Davidson, P.A. & Dalziel, S.B. 2008 Structure formation in homogeneous freely decaying rotating turbulence *J. Fluid Mech.* **598**, 81.

[6] Mininni, P.D. & Pouquet, A. 2010 Rotating helical turbulence. II. Intermittency, scale invariance, and structures *Phys. Fluids* **22**, 035106.

[7] Moisy, F., Morize, C., Rabaud, M. & Sommeria, J. 2011 Decay laws, anisotropy and cyclone-anticyclone asymmetry in decaying rotating turbulence. *J. Fluid Mech.* **664**, 5.

[8] Monin, A.S., & Yaglom, A.M. 1975 *Statistical Fluid Mechanics*, vol. 2 (MIT Press, Cambridge).

[9] Galtier, S. 2009 Exact vectorial law for homogeneous rotating turbulence *Phys. Rev. E* **80**, 046301.

[10] Baroud, C.N., Plapp, B.B., She, Z.S. & Swinney, H.L. 2002 Anomalous self-similarity in a turbulent rapidly rotating fluid *Phys. Rev. Lett.* **88**, 114501.

[11] Morize, C., Moisy, F. & Rabaud, M. 2005 Decaying grid-generated turbulence in a rotating tank *Phys. Fluids* **17**, 095105.

[12] Chakraborty, S. & Bhattacharjee, J.K. 2007 Third-order structure function for rotating three-dimensional homogeneous turbulent flow *Phys. Rev. E* **76**, 036304.

[13] Lamriben, C., Cortet, P.-P., Moisy, F. & Maas, L.R.M. 2011 Excitation of inertial modes in a closed grid turbulence experiment under rotation. *Phys. Fluids* **23**, 015102.

[14] Bewley, G.P., Lathrop, D.P., Maas, L.R.M. & Sreenivasan, K.R. 2007 Inertial waves in rotating grid turbulence *Phys. Fluids* **19**, 071701.